Oceanic Equatorial Waves and the 1991–93 El Niño

WILLIAM S. KESSLER AND MICHAEL J. MCPHADEN

NOAA/PMEL, Seattle, Washington

(Manuscript received 22 June 1994, in final form 30 December 1994)

ABSTRACT

Equatorial Kelvin and Rossby waves associated with the 1991–93 El Niño warm event were detected in temperature observations made by the Tropical Atmosphere-Ocean (TAO) buoy array. Intraseasonal Kelvin waves were a prominent part of equatorial thermocline depth variability and were well represented by a simple model consisting only of first- and second-mode baroclinic Kelvin waves. The second mode was essential to properly represent the observed amplitude. Thermocline depth variability at 5°N and 5°S was dominated by annual and interannual Rossby waves, which were found to have been largely wind forced in midbasin, with little if any signal associated with eastern boundary reflection. An evaluation of the Wyrtki buildup hypothesis and the delayed oscillator hypothesis in connection with the 1991–93 events showed that a long lag (about two years) occurred between the arrival of the downwelling signal in the west and the subsequent initiation of El Niño; this was considerably longer than suggested by delayed oscillator theory. No downwelling Rossby wave reflections occurred at the right time to trigger the onset of the 1991–92 warm event. Termination of the 1991–92 El Niño was due to an upwelling Rossby wave generated during the height of the warm episode, then reflected from the western boundary, consistent with delayed oscillator ideas. However, in early 1993, a second (weaker) warm episode occurred against the background of a very anomalously shallow west Pacific thermocline. This shows that the El Niño–Southern Oscillation cycle cannot be viewed simply as an oscillator mediated by the western boundary reflection of equatorial Rossby waves and that a buildup of a thick warm layer in the west is not a prerequisite to the occurrence of El Niño.

1. Introduction

In this study, we present observations of oceanic equatorial waves during 1988–93 and discuss their role in generating, sustaining, and terminating the 1991–93 El Niño, in light of theories of the El Niño–Southern Oscillation (ENSO) cycle. We will show significant discrepancies between variability observed during 1991–93 and current ideas of the El Niño phenomenon and suggest a need for modification of the related hypotheses known as the "buildup" (Wyrtki 1975) and the "delayed oscillator" (Battisti 1988; Suarez and Schopf 1988). In a companion paper (Kessler and McPhaden 1995, hereafter KM), we have given a description and chronology of the 1991–93 El Niño event and discussed processes controlling central Pacific SST variability during that period.

The present paper is limited by considering only surface wind and upper-ocean temperature observations diagnosed with simple equatorial wave models. This approach does not allow examination of the full coupled complexity of the phenomenon, but the results should nevertheless be useful in evaluating the details of coupled model studies. We focus here on the specific oceanic equatorial waves observed during the 1991–93 El Niño in order to assess the role of the waves in the evolution of the ENSO cycle. Major expansion of the Tropical Atmosphere-Ocean (TAO) buoy array (see next section) began in 1991 as the event got underway, so these waves could be traced with unprecedented accuracy. Although here we discuss only the coupled instability/delayed oscillator view of the ENSO cycle, which provides a clear hypothesis testable against our wave observations, there is an alternative view argued in a series of papers by Penland and collaborators (Penland and Magorian 1993; Penland and Matrosova 1994; Penland and Sardeshmukh 1995). This view suggests that ENSO is not an instability, but could be due to constructive interference of damped, stable SST modes excited by stochastic forcing. These authors have shown some skill in hindcasting interannual variability of east Pacific SST (Penland and Sardeshmukh 1995), but this may be partly due to the fairly regular series of El Niño events in recent years (Battisti and Sarachik 1995). In any case, the observations presented here are not suitable for examination of these larger questions of the stability of the coupled system in the Pacific.

Uniquely among modern El Niño events, after an apparent return to cool conditions in the eastern Pacific in the second half of 1992, another briefer, weaker warm event occurred in boreal spring 1993 (KM). We will use the terms "1991–92 event" to refer to the warm event that began in September 1991, peaked in March

Corresponding author address: Dr. William S. Kessler, NOAA/PMEL/OCRD, 7600 Sand Point Way NE, Seattle, WA 98115.

1992, and returned to cold SST in the eastern Pacific by August 1992, and "1993 event" to refer to the briefer warming in boreal spring 1993. The 1993 event was particularly surprising since an often-stated paradigm for El Niño assumed that warm events are preceded by a year or more of stronger-than-normal trade winds, which build up a thick warm layer in the western equatorial Pacific (Wyrtki 1975). Then, with the onset of El Niño, excess heat content in the western equatorial Pacific is drained by eastward and poleward oceanic heat flux (Wyrtki 1975; Cane et al. 1986; Springer et al. 1990). However, we will show that although the 1991–92 event was preceded by a nearly normal deep western Pacific isothermal layer, the 1993 warm event occurred while the west Pacific thermocline was still quite anomalously shallow.

This paper is organized as follows: section 2 discusses data collection and processing, and section 3 shows variability associated with intraseasonal equatorial Kelvin waves. A simple Kelvin wave model is used to evaluate the contribution of vertical modes and to determine the location of the forcing that produced the thermocline depth anomalies during the El Niño. Section 4 discusses the observations of the 1991–93 event in light of theories of ENSO, focusing in particular on the role of western boundary reflection. Section 5 summarizes the results and gives conclusions.

2. Data description and processing

a. The TAO buoy array

The principal dataset used in this paper is the TAO buoy array, which consists of more than 60 deep-ocean moorings spaced at 2°–3° meridional separation and 10°–15° longitudinal separation across the equatorial Pacific (McPhaden 1993) (Fig. 1). Most of these buoys are Autonomous Temperature Line Acquisition System (ATLAS) thermistor chain moorings (Hayes et al. 1991), which measure temperature at the surface and 10 subsurface depths down to 500 m, as well as surface winds, relative humidity, and air temperature. Air temperatures, relative humidities, and water temperatures are sampled 6 h^{-1}, and daily averages of these are transmitted in real time each day to shore by satellite via Service Argos. Vector winds 3.8 m above the surface are sampled at 2 Hz for 6 minutes each hour and similarly averaged and transmitted. An advantage of the buoy observations is that the nearly continuous sampling virtually eliminates temporal aliasing, which would otherwise be a severe problem in the equatorial Pacific where intraseasonal and higher-frequency variability is prominent. The total number of buoys in operation has climbed from the few that were deployed along the equator in the eastern Pacific in the late 1970s, to about 15 in 1988, then to 20 by mid-1991. Since then the number increased rapidly to more than 60 by mid-1993. Figures 2, 3, and 4 show time–longitude sections of zonal winds, SST, and 20°C depth along the equator linearly interpolated between the buoys, with mooring locations indicated at the edges of each plot. Until late 1991 there were no buoys regularly placed west of 165°E, which is a disadvantage because we would like to examine waves that reflect from the western boundary. For this reason we also make use of expendable bathythermograph (XBT) data described in the next subsection.

b. XBT dataset

The XBT dataset is an outgrowth of the French–American ship of opportunity program (Meyers and Donguy 1980), now collected and quality controlled at the Subsurface Data Centre in Brest, France. Until recently, the TAO buoy network did not extend west of 165°E, so the XBTs are used here to fill in the western boundary region for comparison with model results. The irregularly sampled XBT profiles were binned into 2° latitude by 5° longitude by 2-month

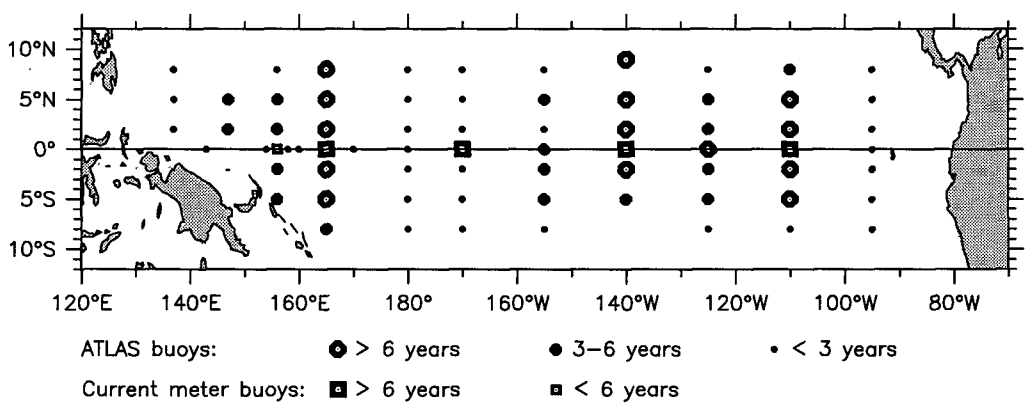

FIG. 1. Map of the TAO buoy network as of September 1993. Round symbols are ATLAS thermistor chain buoys, while square symbols have additional current meters. The size of the symbols indicates the length of time a buoy has been in the water at each location.

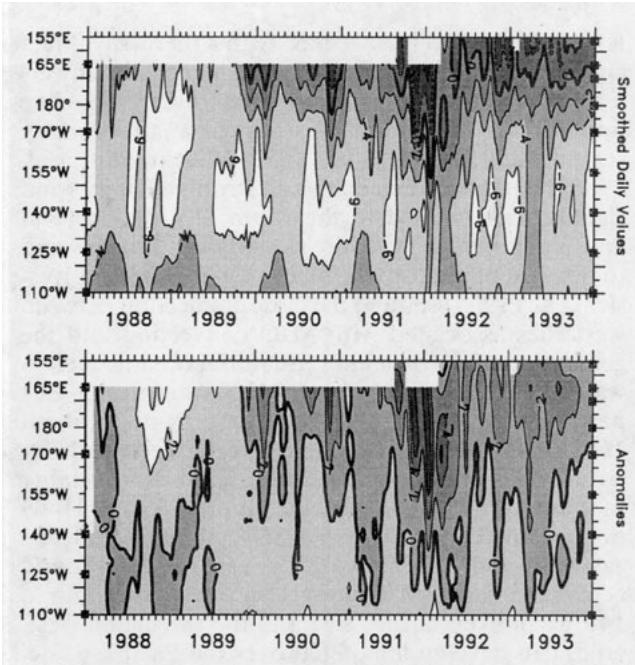

FIG. 2. Zonal wind (m s^{-1}) along the equator during 1988 through 1993, measured by the TAO buoys and smoothed with a 31-day running mean. (Top) Daily values. (Bottom) Anomalies from the COADS annual cycle. Contours and shading levels are every 2 m s^{-1}. Darker shading indicates more positive (westerly) zonal wind. Small squares along the left and right edges of the plot show the positions of the buoys used to make the gridded field at the beginning and end of the study period.

boxes, with an average of about 3.2 profiles per box between 5°N and 5°S during 1988–93. The binned data were smoothed with a 1-2-1 filter twice in longitude and once in time. The relatively sparse sampling means that much of the variability is blurred and aliased compared to the fine resolution of the TAO buoys, nevertheless this dataset is the only means for observing subsurface thermal structure in the far western Pacific during the onset of the 1991–92 event.

c. *The Florida State University wind product*

The Florida State University (FSU) wind product is a monthly compilation of analyzed ship and buoy winds on a 2° by 2° grid over the tropical Pacific (Legler 1991). This dataset has been used to force numerous models of the tropical Pacific (Busalacchi and O'Brien 1980, 1981; Wakata and Sarachik 1991a; Kessler and McCreary 1993; Mantua and Battisti 1994). The TAO buoys (nominally at ±2°, ±5°, and ±8° latitude) are not well placed to calculate the wind stress curl, which has relatively narrow meridional scales in this region, so for the purpose of estimating the off-equatorial forcing on the ocean this supplemental dataset is necessary. We also use the FSU winds to check gross features of the winds to the east and west of the buoy array, recognizing that their monthly resolution blurs the occurrence of intraseasonal and higher-frequency phenomena. Zonal and meridional wind stress components τ^x and τ^y were found from the pseudostress FSU product with drag coefficient $c_D = 1.5 \times 10^{-3}$.

d. *Climatologies: COADS (wind), satellite-blended product (SST), historical XBT compilation (20°C depth)*

Climatologies from a variety of sources were used to define anomalies of observed quantities. For surface zonal wind speed, anomalies were found from the Coupled Ocean–Atmosphere Data Set (COADS) average annual cycle for the period 1946–89. COADS is a monthly compilation (extending back into the 1800s) of surface meteorological observations from ships, binned on a global 2° by 2° grid (Woodruff et al. 1987). SST anomalies were defined relative to the average annual cycle based on the most recent 10 yr of the Reynolds and Smith (1994) blended satellite product. This is a weekly product that uses surface observations (including the TAO buoys) to reference satellite Advanced Very High Resolution Radiometer measurements. Anomalies of 20°C isotherm depth were estimated from a climatology based on XBT/MBT (mechanical bathythermograph) data compiled by Kessler (1990), consisting of 21 811 profiles between 5°N and 5°S taken during 1970 to 1987. The terms "normal,"

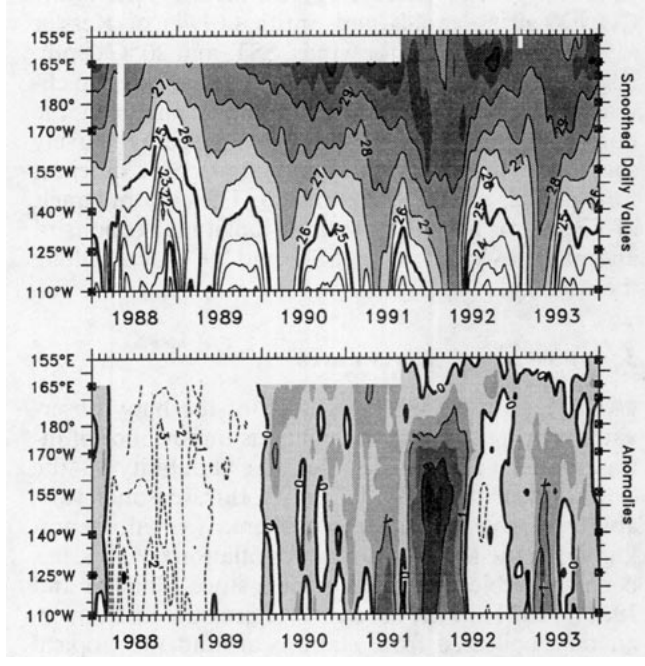

FIG. 3. As Fig. 2 except SST (°C), smoothed with a 31-day running mean. Top: Daily values. Bottom: Anomalies from the Reynolds and Smith (1994) annual cycle. Contours are every degree Celsius. For the observed values, shading indicates SST greater than 26°C, with a shading levels every 1°C and a supplemental shading level to indicate 29.5°C. For the anomalies, shading indicates SST warmer than climatology, with shading levels every 0.5°C and contours every 1°C.

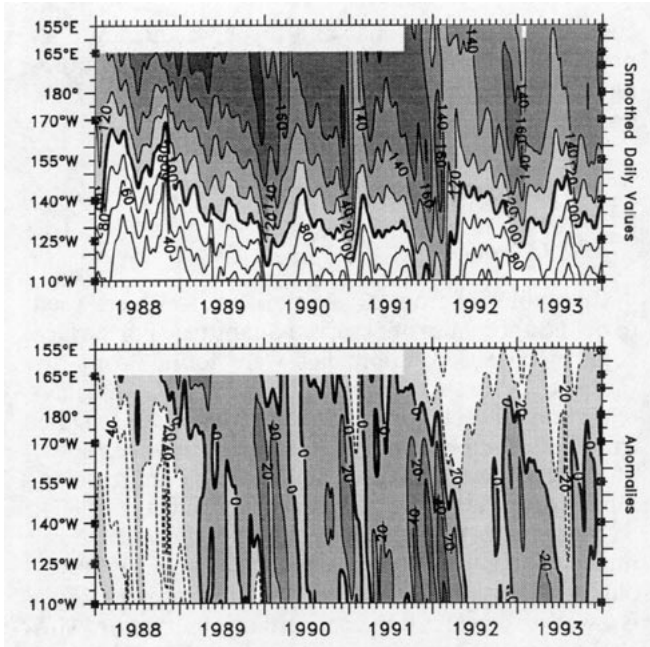

FIG. 4. As Fig. 2 except 20°C depth (m), smoothed with a 15-day running mean. Top: Daily values. The contour interval is 20 m. Shading indicates isotherm depth greater than 100 m. Bottom: Anomalies from the annual cycle derived from XBT data. Shading indicates anomalies deeper than −20 m (positive values are deeper than climatology).

"anomaly," and "climatology" in the text refer to the COADS or Reynolds and Smith (1994) or Kessler (1990) annual cycles for winds, SST, and 20°C depth, respectively. We have chosen to use these external climatologies rather than constructing them from the buoy data itself, since most buoy records are relatively short (less than 10-yr duration) and cover different time periods at different locations. The bottom panels of Figs. 2, 3, and 4 show time–longitude sections of anomalies of zonal winds, SST, and 20°C depth along the equator.

3. Intraseasonal Kelvin waves

The high temporal resolution of the buoy observations brings out the conspicuous importance of intraseasonal (30–100 day period) variability in the evolution of the 1991–93 event. Intraseasonal variability of the tropical atmosphere, a phenomenon known as the Madden–Julian oscillation (MJO), has been the subject of many papers since Madden and Julian (1971, 1972) used surface pressure and upper-air data collected from stations around the tropical belt to show that these fluctuations were of global scale and had aspects suggesting an eastward-propagating wave. The MJO usually arises over the central Indian Ocean as an organized region of deep convection. As the convection intensifies, it moves east at speeds of 3–6 m s^{-1} (Rui and Wang 1990; Weickmann and Khalsa 1990) and is associated with a thermally direct circulation in the equatorial zonal plane, with lower-level convergence and upper-level divergence. The upper-level wind anomaly pattern grows to planetary scale (Madden and Julian 1972; Weickmann et al. 1985), but deep convection and strong westerly wind signals are restricted to the warm SST region (Rui and Wang 1990). Typically westerly winds below and to the west of the convection can be intense, and Kessler et al. (1995) showed the close connection between westerlies associated with MJO convection and the generation of downwelling equatorial oceanic Kelvin waves in the Pacific. As each MJO event moves east past the edge of the west Pacific warm pool (about 160°E–180°), its convection and surface wind signature become very weak, so intraseasonal variability in the eastern Pacific is usually remotely forced. However, during El Niño, as warm SST anomalies progress eastward and SST above 28°C can often be found across the basin, MJO convection may penetrate to 140°W or even farther east and the associated westerlies can develop long fetch over the Pacific, as occurred in early 1992 (KM).

The intraseasonal Kelvin waves constituted one of the most prominent features of subsurface temperature and zonal current variability during the 1991–93 El Niño (KM). The slow eastward propagation of anomalies across the equatorial Pacific that took place in the last months of 1991 (Figs. 2, 3, and 4) was found to have occurred as a series of steps modulated by the occurrence of MJOs and the resulting intraseasonal waves. Four of these waves occurred during the onset phase of the warm event at the end of 1991: in August–September and again in November 1991, and in January and March 1992 (visible as the dark bands in Fig. 4). In section 3a we develop a simple model of wind-forced Kelvin waves and then in section 3b discuss its representation of the observed fluctuations of 20°C depth.

a. A Kelvin wave model

The importance of intraseasonal Kelvin waves to the evolution of the thermocline at 140°W during 1991–93 can be demonstrated by a simple model that includes only the effects of winds in the interior of the basin generating Kelvin waves. A solution is found using the method of Gill and Clarke (1974), integrating the winds along the Kelvin wave characteristic $(x-ct)$ = constant. This can be expressed as a sum over vertical baroclinic modes, each of which is an integral over the winds along the path of the wave

$$A(x_0,z,t)=\sum_{n=1}^{\infty}A_n(x_0,z,t)$$

$$=\sum_{n=1}^{\infty}\alpha_n(z)\int_{165°\mathrm{E}}^{x_0}\tau^x\left[x,t+\frac{(x-x_0)}{c_n}\right]dx, \quad (1)$$

where A_n is the baroclinic mode-n Kelvin part of the ocean signal for various quantities (discussed below) with corresponding coefficients α_n, τ^x is the zonal wind stress, and c_n is the long gravity wave speed for mode n. The sum is over the baroclinic modes of the system. The z-dependence is through the vertical structure functions $\Psi_n(z)$ of the baroclinic modes, which form an orthogonal and complete set (McCreary 1981). Both c_n and $\Psi_n(z)$ depend on the mean density profile and the depth of the ocean and are determined by solution of a Sturm–Liouville eigenvalue problem; the $\Psi_n(z)$ are normalized as in Cane (1984). The mean density profile used here was obtained from the average of 43 equator crossings over 16 months during the Hawaii–Tahiti Shuttle experiment at 150°–158°W (Wyrtki and Kilonsky 1984); Table 1 gives values for the modal parameters for the first four baroclinic modes.

The wind stress τ^x was calculated from daily buoy wind velocity components adjusted to 10-m height assuming neutral stability, with a constant drag coefficient $c_D = 1.3 \times 10^{-3}$ and air density 1.2 kg m^{-3}. The winds were linearly interpolated in longitude between buoy locations (Fig. 2) and smoothed with a triangle filter of total width 5 days (half power at about 6-day periods). We assume that the equatorial wind measurement represents a wind field sufficiently wide in the meridional direction (one Rossby radius or about 350 km for the first baroclinic mode) to project fully onto the Kelvin mode (Cane 1984). The integration was started at 165°E, where the western boundary condition was taken to be zero, so the solution expresses only the result of interior ocean wind forcing of vertical mode n Kelvin waves. The choice of boundary condition omits effects of variability forced further to the west or reflected from the western boundary. Other types of waves, mixing processes, advection, etc. are also excluded from the model.

Solutions to (1) can represent any of the quantities zonal current, pressure, density, or isopycnal displacement, depending on the form of coefficients α_n. This generality expresses the fact that all the Kelvin wave variables have the same phase and structure in (x, y, t), differing only by an amplitude factor, and in some cases their vertical dependence. Sea level variations due to mode n are found from (1) using $\alpha_n^{SL} = \Psi_n(0)^2/\rho g D$, where ρ is the density of seawater, g is gravity, and D is the full depth of the ocean. Zonal current and pressure variations of each mode are functions of depth, with coefficients $\alpha_n^U(z) = \Psi_n(0)\Psi_n(z)/\rho c_n D$ and $\alpha_n^P(z) = \Psi_n(0)\Psi_n(z)/D$, respectively. A multiple mode solution can be derived that is comparable to observed 20°C depth variability; in this case isopycnal displacements due to each mode can be found using the coefficient

$$\alpha_n^{20°C}(z_i) = \frac{\Psi_n(0)}{gD} \frac{d\Psi_n(z_i)/dz}{d\rho_b(z_i)/dz}, \qquad (2)$$

where the vertical gradients of the structure functions $\Psi_n(z)$ and the background density $\rho_b(z)$ are evaluated at the mean depth z_i of the isopycnal to be studied (in this case at $z_i = 125$ m for 20°C depth). The calculation assumes that vertical displacements are small relative to the vertical scale of the background density profile. There may be times when this assumption is questionable since the observed depth of 20°C varies between 80 and 180 m; nevertheless, as we will show, the comparison between observed and modeled fluctuations is generally good.

Table 1 gives values for coefficients α_n of quantities represented by (1) for the first four baroclinic modes, based on the central Pacific mean profile. For sea level (or equivalently surface pressure), the α_n decrease monotonically with increasing mode number, indicating that mode 1 tends to dominate. However, this amplitude relationship for sea level cannot be generalized to other variables. For example, mode 2 coefficients α_2 for surface zonal current and isopycnal displacement at thermocline level are larger than those of mode 1. In the case of isopycnal displacement at thermocline level, the larger amplitude of

TABLE 1. Values of baroclinic mode parameters for the first four modes, calculated from the mean equatorial density profile obtained during 46 equator crossings of the Hawaii–Tahiti Shuttle experiment. Also, values of the Kelvin wave coefficients α_n used to evaluate the Kelvin wave integration (1) are shown.

	1	2	3	4
Equivalent depth H_n (cm)	76.0	30.9	11.5	5.9
Surface amplitude Ψ_n (0)	4.29	3.90	1.70	1.25
Wave speed $c_n^2 = gH_n$ (m s^{-1})	2.73	1.74	1.06	0.76
Timescale $(\beta c_n)^{-1/2}$ (days)	1.47	1.84	2.35	2.78
Rossby radius $(c_n/\beta)^{1/2}$ (km)	346	276	216	183
ULT analogue H (m)	244	295	1561	2893
$\Delta\rho/\rho$ analogue ($\times 10^3$)	3.11	1.05	0.073	0.020
Values of coefficients α_n in Eq. (1):				
Sea level ($\alpha_n^{SL} \times 10^3$) (m s^2 kg^{-1})	4.08	3.38	0.64	0.34
Surface zonal speed ($\alpha_n^U \times 10^6$) (m s kg^{-1})	1.47	1.90	0.59	0.44
Isopycnal depth, $z = 125$ m ($\alpha_n^{20°C} \times 10^5$) (m s^2 kg^{-1})	6.02	11.51	4.85	3.77

α_2 is due to the strong vertical gradient of Ψ_2 at that depth [q.v. Eq. (2)].

A common model formulation is the reduced gravity or 1½-layer system, which can also be expressed in the form (1), with the sum over n modes replaced by a single coefficient $\alpha_{1\,1/2}$, representing upper-layer thickness anomalies (ULTA) (e.g., Busalacchi and O'Brien 1981). The ULTA coefficient is $\alpha_{1\,1/2} = (\rho c_{1\,1/2}^2)^{-1}$, which depends only on the choice of reduced gravity phase speed $c_{1\,1/2}$, a relatively well-defined quantity. Zonal velocity and sea level anomalies associated with the reduced gravity solution have coefficients $\alpha_{1\,1/2} = (\rho c_{1\,1/2} H)^{-1}$ and $\alpha_{1\,1/2} = \Delta\rho/\rho^2 c_{1\,1/2}^2$, respectively, and depend on the additional choices of mean upper-layer thickness H and density difference $\Delta\rho$ between the upper and lower layers. Cane (1984) showed that the reduced gravity and baroclinic mode solutions can be made equivalent by defining the 1½-layer parameters $H = D/\Psi_n(0)^2$ and $\Delta\rho/\rho = (c_n\Psi_n(0))^2/gD$ (see Table 1 for values). However, one can also consider any two of c, H, and $\Delta\rho$ [where $c_{1\,1/2} = (gH\Delta\rho/\rho)^{1/2}$] to be free parameters in a representation of the ocean as two homogeneous layers, which is distinct from a single baroclinic mode of a continuously stratified fluid. For example, Rebert et al. (1985) and Kessler and Taft (1987) used regression fitting against 20°C depth to find the value of $\Delta\rho/\rho$, which gave the best representation of geostrophic currents and sea level in the tropical Pacific. Busalacchi and O'Brien (1980, 1981) chose H = 200 m and 300 m, with c = 2.0 m s^{-1} and 2.45 m s^{-1}, respectively, in two model studies of wind-driven variability. We will show that during 1991–93 at 140°W, reasonable parameter choices can be made so that the 1½-layer formulation reproduces observed 20°C depth fluctuations as well or better than a multiple-mode model.

Figure 5 shows the observed time series of 20°C depth at 140°W during 1991–93 compared to four different hindcasts made using (1). First, Fig. 5a gives solutions representing isopycnal displacement at the mean depth of 20°C, with α_n defined by (2), for the first and second baroclinic modes separately. As expected from the relative size of the coefficient α (Table 1), the second baroclinic mode solution was larger than the first (rms amplitude 9.96 m for the second mode compared to 5.79 m for the first) during 1991–93. The phases of the two modal solutions were quite similar because much of the forcing occurred between 180° and 140°W (Fig. 2), so there was little time for the modes to separate zonally. It would take the first (second) mode 18.9 (29.6) days to travel from 180° to 140°W; correlation between the two modes was largest (0.93) when the second mode lagged the first by 8 days (consistent with an average forcing location at about 170°W), but it was still quite high (0.83) at zero lag. Even at 110°W correlation between modes 1 and 2 was fairly large (0.76) at zero lag. Figure 5a shows the

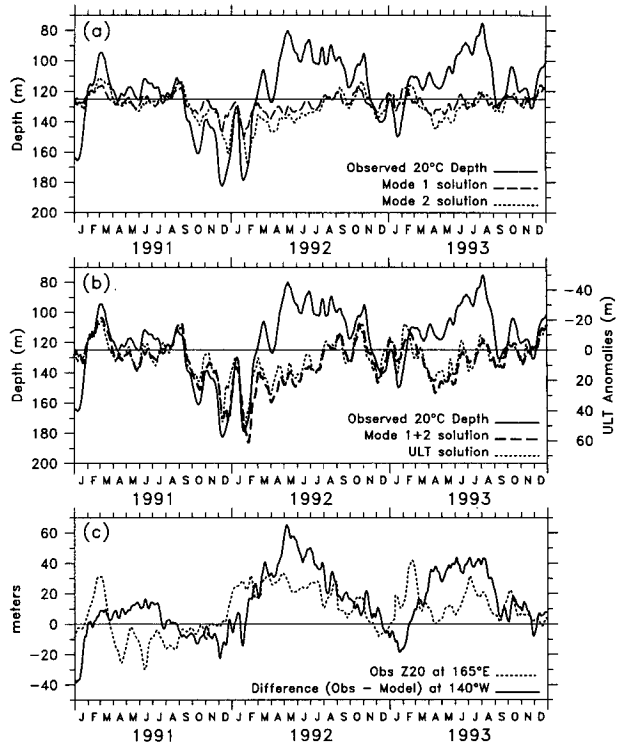

FIG. 5. Solutions to the Kelvin wave model (1) compared to observed 20°C depth at 140°W. (a) Observations (line) and solutions representing isopycnal displacement for the first (dash) and second (dot) baroclinic modes separately. (b) Observations (line) and isopycnal displacement solutions for the sum of modes 1 and 2 shown in Fig. 5a (dash) and for upper-layer thickness anomalies by the 1½-layer reduced gravity formulation (dot; scale at right). (c) Difference between the isopycnal displacement solution shown in Fig. 5b minus the demeaned observations (solid line; scale at left), plotted so positive values indicate the model solution is too deep. The dotted line shows the anomalies of thermocline depth at 0°, 165°E observed at the buoy there, lagged by 30 days to account for Kelvin wave propagation to 140°W. The shoaling seen at 165°E in early 1992 would tend to correct a large part of the discrepancy at that time.

slight delay between the two solutions. Therefore it is very difficult to distinguish between modes on the basis of phase lag. However, neither mode alone had sufficient amplitude to properly represent the observed variability (Fig. 5a), and a realistic simulation requires a sum over at least two modes. In contrast, modes 3 and 4 had rms amplitudes of 3.67 m and 2.82 m, respectively (roughly half that of mode 1), and much lower correlation with the observations (r_1 = 0.91 and r_2 = 0.77, while r_3 = 0.51 and r_4 = 0.57, during August 1991–February 1992). These higher modes can reasonably be neglected when comparing model results to observations.

Figure 5b shows the solution summing the first two modes and also the reduced gravity solution representing ULTA, where $c_{1\,1/2}$ has been chosen to be 2.73 m s^{-1}, the same as the first baroclinic mode speed. The ULTA solution represents anomalies and thus has

arbitrary placement along the vertical axis (for Fig. 5b we use H = 125 m, corresponding to the mean depth of 20°C), unlike the isopycnal displacement solution, which is fixed in the vertical during the evaluation of Eq. (2). The isopycnal displacement solution summing two baroclinic modes retains more of the dynamics than the simpler reduced gravity ULTA, and earlier models (Busalacchi and Cane 1985; Giese and Harrison 1990) and observational (Lukas et al. 1984) studies have suggested a role for second baroclinic mode Kelvin waves during the onset of El Niño. However, these two hindcasts appear nearly identical (Fig. 5b) and have correlation 0.93 during 1991–93. The ULTA solution, in fact, gave a somewhat better representation of the observations, with slightly higher correlation and rms difference with the observations about 20% smaller (10.7 m for the modes 1 + 2 solution and 8.6 m for the reduced gravity formulation).

The correspondence between the reduced gravity and vertical modal sum solutions shown in Fig. 5b may be another reason why many investigators have had success working with reduced gravity models to interpret variability in the equatorial Pacific (e.g., Busalacchi and O'Brien 1981), even though the second mode has large amplitude in thermocline depth. The similarity of the two solutions indicates that it is possible to choose reduced gravity parameters and closely simulate the effect of multiple modes, if the forcing is not too far away and the modes do not have sufficient time to disperse. By choosing the first baroclinic mode phase speed (c_1 = 2.73 m s^{-1}) for the reduced gravity formulation, and then taking the results of (1) to apply at the level of 20°C depth (about 125 m), we have in effect artificially increased the amplitude of the first mode solution, which properly should be analogous to a reduced gravity system with mean upper-layer thickness $H = D/\Psi_1(0)^2$ = 244 m in this case (Cane 1984). Nevertheless, these choices of c and H are quite reasonable if one regards the equatorial Pacific as equivalent to two homogeneous fluids with their interface at the depth of the 20°C isotherm. The result is that the two distinct model formulations arrive at very similar solutions (Fig. 5b). However, the modal decomposition shows that both first and second modes are essential to properly represent thermocline displacements associated with the Kelvin waves. The reduced gravity technique, while very much simpler to apply, might lead to an erroneous interpretation in terms of the amplitude, timing, and vertical structure of wind-forced variability in a situation where the forcing was distant and the modes separated.

b. *Dynamical interpretation*

The correlation between modeled (two-mode isopycnal displacement) and observed 20°C depth time series at 140°W (Fig. 5b) is 0.86 for January 1991 through February 1992 and 0.46 for the entire 1991–93 period. Differences between the model solution and observed 20°C depth variability are shown in Fig. 5c. The corresponding correlations at 110°W are 0.91 and 0.55 and the agreement is similar to that shown in Fig. 5b. For the onset phase of the warm event (up to the thermocline depth maximum at the end of January 1992), clearly the great bulk of thermocline depth variability in the east-central Pacific was due to Kelvin waves generated in the interior Pacific east of 165°E, with differences on the order of 10 m or less (Fig. 5c). Both the intraseasonal downwelling pulses and the lower-frequency deepening are well represented by the simple model and were due to westerlies extending into the central basin (Fig. 2). Apparently no significant influence of thermocline depth variability from west of 165°E (or reflected from the western boundary) was part of the onset stage.

A very different conclusion is gleaned from the model results for the termination phase of the 1991–92 event, when the observed central Pacific thermocline shoaled about 100 m, reversing the earlier deep anomalies (Fig. 5a). This signal was not expressed in the model solutions, and model minus observation differences increased to more than 60 m (Fig. 5c). Clearly the strong shoaling of the thermocline at 140°W during early 1992 was not associated with interior wind-forced Kelvin waves, either of the first or higher vertical modes. The large discrepancy indicates that the ocean at 140°W was being affected by other processes than are encompassed in (1).

A reasonable hypothesis for the thermocline shoaling observed in mid-1992 might be that upwelling forced by local winds at 140°W controlled thermocline variations during this period. However, these winds were near normal or slightly anomalously westerly at the time (Fig. 2, bottom), and so could not have been the explanation for the observed upwelling. Near-normal winds also occurred east of 140°W during 1992 (Fig. 2), so the observed thermocline shoaling was unlikely to have been due to Rossby waves arriving at 140°W. Probably the major missing element in (1) is the contribution of forcing occurring west of 165°E, evident in the roughly 30 m shoaling of the thermocline at 165°E during early 1992 (Fig. 5c), which would tend to raise the thermocline at 140°W at about the right time to improve the comparison. It is not straightforward, however, to include this variability in a model as simple as (1), since part of the 165°E signal is due to westward propagating Rossby waves (see next section), and thus not all of those fluctuations can be taken as an ordinary boundary condition for Eq. (1). We will return to this question in section 5.

c. *Eastern boundary reflection of intraseasonal Kelvin waves*

Before going on to interannual Rossby waves (following section), it is appropriate to consider whether

the prominent intraseasonal Kelvin waves discussed in this section produce intraseasonal Rossby waves coming back into the central basin following reflection from the eastern boundary. There is no question that intraseasonal Kelvin waves reach the eastern boundary; Spillane et al. (1987) and Enfield (1987) showed a clear connection between the equatorial intraseasonal waves and coastal Kelvin waves, which could be observed as far north as San Francisco. At 60-day periods, free equatorial Rossby waves up to meridional mode 5 exist (for the first baroclinic mode), so such reflected waves are possible. Spectral analysis of thermocline depth at locations along 5°N and 5°S yields a weak signature of 60-day variability. However, examination of the coherence of intraseasonal energy off the equator shows that these signals propagated east at the Kelvin wave speed, and are thus simply the extension of the equatorial anomalies, not a Rossby reflection. No evidence of westward-propagating intraseasonal variability was seen in the buoy temperature records.

Linear equatorial wave theory offers three possible rationalizations as to why we should not expect to observe reflected intraseasonal waves in the buoy time series. First, Clarke (1983, 1992) has shown that significant incoming Kelvin wave energy is lost due to coastal trapping. Lower reflectivity occurs for higher frequencies, higher vertical modes, and nonmeridional eastern boundaries. The energy flux reflection coefficient for 60-day, first-baroclinic-mode Kelvin waves on a meridional eastern boundary is about 0.50 (Clarke 1983); for a realistic American coast this is reduced to about 0.47 (A. J. Clarke 1994, personal communication). Second, Schopf et al. (1981) showed that periodic Rossby waves emanating from the eastern boundary propagate along ray paths that, for a single baroclinic mode, are sinusoidal about the equator. These rays have focal points on the equator at $x = -(2n - 1)\pi c/4\omega$, $n = 1, 2, 3, \ldots$ (for 60-day period, first baroclinic mode waves the first focal point is 1555 km west of the coast, or about 94°W in the Pacific). Chang and Philander (1989) have also shown that in the region of the North Equatorial Countercurrent (4°–10°N) Rossby ray paths would be distorted by the mean zonal currents to propagate even more rapidly toward the equator. At these focal points wave rays converge; the WKB wavelengths become short and the amplitudes large, so even small dissipation would be sufficient to damp them rapidly (Schopf et al. 1981; Kessler 1989). A third possible reason for why we do not observe 60-day Rossby waves reflected from the American coast is that if more than one vertical mode is involved, then the sum over modes leads to vertically propagating ray paths (with no focal points) (McCreary 1984). The reflected Rossby waves would propagate vertically into the deep ocean, with a slope proportional to frequency (McCreary 1984; Kessler and McCreary 1993). For the mid-Pacific stratification used in the modal calculation above, 60-day first-meridional-mode Rossby waves would propagate quite steeply, reaching the ocean bottom 22° of longitude west of the coast; higher meridional-mode waves would propagate even more steeply. For these reasons, our failure to observe any expression of intraseasonal Kelvin waves reflecting off the American coast and propagating as Rossby waves along the 5°N buoy line is not surprising.

4. The buildup, the delayed oscillator, and the El Niño of 1991–93

a. Introduction

A consistent element of theories for the development of El Niño has been the idea that the west Pacific warm pool is the crucible for the onset of warm events. Wyrtki (1975) noted that the El Niño warming, which had long been known in the eastern Pacific, could not be explained by changes in the local or regional winds. He hypothesized that during the years preceding the warm event stronger than normal trade winds "build up" a thick warm layer in the west that provides the potential for a downgradient eastward flow along the equator once the winds relax. This eastward flow was then thought to bring the excess warm water back to the eastern Pacific in a warm event (El Niño). The Wyrtki theory was the first that explicitly identified the west Pacific warm pool as crucial to the triggering of El Niño; earlier ideas (Bjerknes 1966) had recognized that El Niño was a basinwide phenomenon, but without specific reference to the dynamics of a bounded equatorial ocean.

As we have come to understand the mechanisms by which midbasin wind signals generate Rossby waves that propagate to the western boundary and reflect to return along the equator as equatorial Kelvin waves (Moore and Philander 1977; Godfrey 1975; Cane and Sarachik 1977; Clarke 1983; Cane and Gent 1984), theories of El Niño have been developed that exploit the time lag associated with wave propagation to attempt to explain the quasi-periodic nature of ENSO. Two ideas that are at the heart of many of the subsequent El Niño oscillator models were first suggested by McCreary (1983): the time-lagged negative feedback through reflection from the western boundary, and the control of equatorial winds by a simple parameterization of SST in terms of thermocline depth. At their most basic, these mechanisms work together as follows. Eastern equatorial Pacific SST is assumed to be warm when the thermocline is deep and cool when it is shallow. Equatorial winds are assumed to be anomalously westerly when east Pacific SST is warm and anomalously easterly when it is cool. Thus, say, when the east Pacific thermocline is shallow and SST cool, easterly winds prevail. The easterlies produce downwelling of the thermocline north and south of the equator and a westward equatorial jet. These signals propagate west as a Rossby wave and reflect from the western boundary as downwelling equatorial Kelvin waves. The Kelvin

waves carry the downwelling signal back to the east Pacific region, where they lower the thermocline, warm the SST, and produce anomalous westerly winds, thereby reversing the initial situation. In this manner the system oscillates between warm and cold states. In the original McCreary (1983) model, this process was cyclic, with a timescale set by the meridional structure of the equatorial winds, which determined the latitude of the main forcing region of the Rossby waves and hence their propagation speed. A weakness of this formulation is that in order to get a realistic ENSO timescale (several years) from wave propagation alone, the wind patches had to extend quite far off the equator in order to generate sufficiently slow Rossby waves (Battisti 1989). Philander et al. (1984) and Anderson and McCreary (1985) showed that with a more sophisticated, dynamically constrained atmosphere (as opposed to the fixed-region on–off winds of McCreary 1983) and a more realistic ocean (including mean zonal SST gradients), coupled instabilities could develop in which initial equatorial perturbations grow by interaction between thermocline depth and the asymmetric response of the atmosphere to a heat source (Battisti and Hirst 1989; Clarke 1994).

During the past 10 years, the fundamental ideas proposed in the simple McCreary (1983) and Philander et al. (1984) models have been developed and enlarged upon in a series of coupled model studies that demonstrate "delayed oscillator" physics (Zebiak and Cane 1987; Suarez and Schopf 1988; Battisti 1988; Battisti and Hirst 1989; see the review by McCreary and Anderson 1991). Improvements to the physics in these models include fully nonlinear thermodynamics in the ocean surface layer, which allows SST changes by horizontal advection, upwelling, and heat fluxes to the atmosphere. The atmosphere is driven by latent heat release with contributions from both SST-induced evaporative physics and dynamically controlled atmospheric moisture convergence. These new models establish two additional elements of the coupled interaction. First, instead of the simple pattern of western boundary reflection acting as a switch, the delayed oscillator mechanism provides that the reflected Kelvin waves only slowly erode the existing thermocline anomalies, so that for a time this remotely forced negative feedback mechanism and local winds are in competition. Second, a coupled instability develops in the central basin, in which a depressed thermocline produces anomalous SST warming due to upwelling acting on a weakened vertical temperature gradient, then the warm SST results in anomalous westerly winds over and to the west of the warm patch, which further lowers the thermocline, and the anomaly grows (Yamagata 1985; Battisti 1988; Wakata and Sarachik 1991b). Kelvin waves carry the downwelling eastward, but propagation of the coupled anomaly is slower than the free Kelvin wave speed. These two elements have the effect that a slow (ENSO) timescale can be produced solely within the equatorial waveguide, involving only the first meridional mode Rossby wave and the Kelvin wave, without the need for the unrealistically wide meridional wind structures required by the original McCreary formulation. One no longer expects a warm event to be triggered directly by the Rossby to Kelvin reflection; rather, the reflected wave lowers the thermocline and sets up the coupled instability in midbasin, which then grows with its own timescale, generates its own westerly winds, and produces additional Kelvin waves that reinforce the growing anomaly.

The delayed oscillator is similar to Wyrtki's buildup hypothesis in several essential respects. Both postulate that the period before the onset of ENSO is characterized by anomalously strong easterly winds, with the result that the western equatorial Pacific thermocline becomes anomalously deep. Wyrtki envisaged a quasi-equilibrium balance in which easterlies support a stronger than normal zonal pressure gradient, whereas the delayed oscillator is a time-dependent balance where easterlies generate downwelling equatorial Rossby waves, but the outcome is similar in both cases. During the height of El Niño, both mechanisms see the central Pacific westerlies resulting in a draining of the west Pacific warm pool; Wyrtki pictures a "sloshing back" as the winds can no longer support the pressure gradient, while delayed oscillator theory interprets the flattening of the thermocline slope in terms of a downwelling Kelvin wave going east and an upwelling Rossby wave going west, both involving eastward flow on the equator.

Wakata and Sarachik (1991a) examined the delayed oscillator mechanism by forcing a reduced gravity linear ocean model with observed (FSU) winds. Their goal was to determine whether wind-forced oceanic waves had the correct timing expected by delayed oscillator theory. They found that each of the El Niños between 1961 and 1987 (seven events in 28 years) were preceded by a downwelling gravest meridional-mode Rossby wave forced by enhanced central Pacific trade winds about one year before. The downwelling waves reflected from the western boundary and triggered the warm events. Each of the warm events was terminated by the same process with reversed sign. They therefore concluded that the delayed oscillator mechanism was consistent with the observed events (Wakata and Sarachik 1991a).

b. Model description

We now seek to perform a similar evaluation for the El Niño of 1991–93. Rather than use a complete model of equatorial ocean waves as did Wakata and Sarachik (1991a), our approach will be to first verify that low-frequency variations along 5°N and 5°S are reasonably consistent with a long Rossby wave model forced by observed Ekman pumping and then compare the timing of the downwelling Rossby wave relative to the

occurrence of the warm event. The model integrates observed wind stress curl along 5°N and 5°S to find solutions to the low-frequency quasigeostrophic vorticity equation

$$h_t - \left(\frac{\beta c^2}{f^2}\right) h_x + Rh = -\text{curl}\,\frac{\tau}{\rho f}, \qquad (3)$$

where h is the upper-layer thickness anomaly due to wind forcing and Rossby wave propagation, f is the Coriolis parameter and β its meridional derivative, c is the long gravity wave (Kelvin) speed, R is a damping time taken to be (3 months)$^{-1}$, τ is the wind stress derived from the FSU monthly wind product, and ρ the density of seawater. The long Rossby speed $c_r = \beta c^2/f^2$ equals 0.81 m s^{-1} at ±5° latitude and is approximately equal to the first meridional mode Rossby speed $c/3$. Equation (3) was solved by integrating along long Rossby wave characteristics (the time step was 7 days) analogous to the procedure used for the Kelvin wave model (1). The model solution was adjusted to match the buoy time series of 20°C depth at 5°N and 5°S, 110°W, effectively a boundary condition that influences the results only slightly (the amplitude of model variability in the western Pacific was much larger than the observed variability at 110°W, so the effect of the boundary condition is small). The choice of damping time R is based on the best fit to observed 20°C depth and is consistent with the results of Picaut et al. (1993), who examined the dependence of a wind-forced long-wave model to variation of the damping coefficients. As has been previously noted, such models produce exaggerated amplitudes in the off-equatorial western Pacific (Kubota and O'Brien 1988; Kessler 1991), and the present solution overestimates pycnocline amplitudes in the west. Kessler and McCreary (1993) attributed this discrepancy to leakage into the subthermocline ocean, a process that is excluded from this reduced gravity model. The relatively short damping time is a crude way to deal with this problem. The results of the integration carried out for the period 1961–93 correspond closely to the Rossby waves found by Wakata and Sarachik (1991a), using their much more sophisticated equatorial model.

Although the simple quasigeostrophic model (3) might seem to be inappropriate at low latitude, the results are ex post facto found to be equivalent to what would be seen in an equatorial model based on the meridional structure functions (Moore and Philander 1977). This is evident in that the solutions (shown in Figs. 6a and 6b, top) are nearly symmetric about the equator (correlations between solutions at 5°N and 5°S were above 0.7 everywhere west of 150°W; see for example Fig. 7) and represent disturbances traveling at the speed of a first-meridional-mode equatorial Rossby wave. The reason for the symmetry is that the wind stress curl anomalies that were used to force (3) were primarily due to equatorial zonal winds associated with a quasi-symmetric curl field at ±5° latitude. Of the two components of curl(τ/f), the $\beta\tau^x/f^2$ term (which is the same term as would be used to force an equatorial mode model) was found to be larger than the curl$(\tau)/f$ term both at 5°N and 5°S. The quasigeostrophic formulation (3) has been previously used to successfully diagnose low-frequency variability as close to the equator as 4°N (Kessler 1990) and is exploited here on the basis of simplicity of application. The simplicity of the model also functions as a dynamical filter in that the results display purely the long Rossby part of the physics. Model solutions are com-

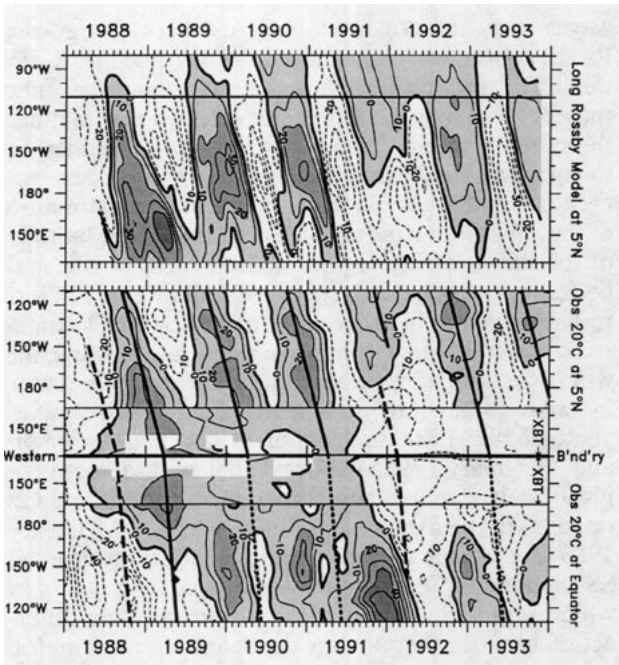

FIG. 6a. Observed and modeled 20°C depth (meters) along 5°N and the equator. All quantities shown are monthly averages demeaned by the 1988–93 mean at each location, and all plots are at exactly the same scale. East is at the top of the two upper panels, but the lower panel has west at top to show wave reflection at the western boundary. (Top) Solution (pycnocline depth) of the long Rossby balance (3) at 5°N, forced by observed (FSU) winds. Contours are every 10 m, with a supplemental contour at 5 m; shading indicates positive (deep) anomalies. The horizontal line at 110°W bounds the region where corresponding 20°C depth data is available for comparison (middle panel). (Middle) Observed depth of the 20°C isotherm along 5°N. Buoy data is used between 110°W and 165°E and XBT data in the far west; a horizontal line divides these regions. The heavy slant lines show the occurrence of deep thermocline anomalies, with the slope indicating the long Rossby propagation speed ($c_r = \beta c^2/f^2 = 0.81$ m s^{-1}). The dashed slanted lines show the occurrence of identified shallow interannual Rossby waves. The heavy line at 130°E separating the middle and lower panels is the western boundary. (Bottom) As in the middle panel, except observed depth of the 20°C isotherm along the equator. The slant lines indicate the equatorial Kelvin waves that would be expected from western boundary reflection of the Rossby waves in the middle panel. Their slope indicates the propagation speed of equatorial Kelvin waves ($c = 2.4$ m s^{-1}). Solid lines are downwelling Kelvin waves, dashed lines are upwelling Kelvin waves, and dotted lines are downwelling Kelvin waves that would have been predicted by western boundary reflection but were not observed.

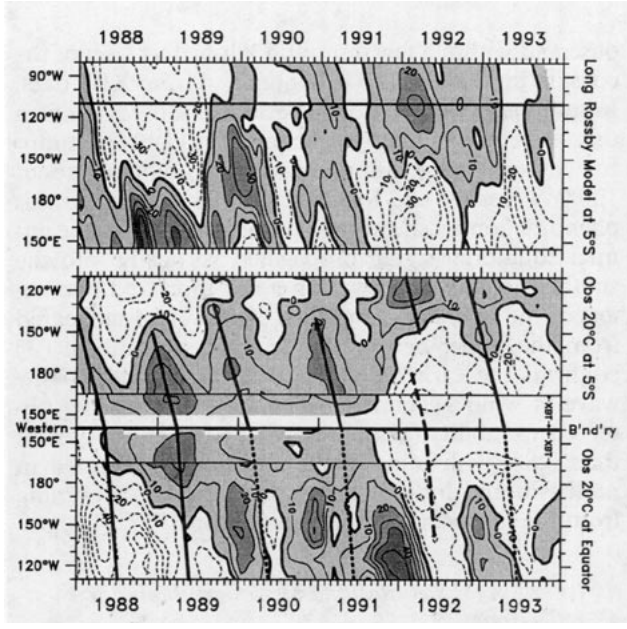

FIG. 6b. As Fig. 6a but at 5°S. The lower panel (observed 20°C depth on the equator) is the same as in Fig. 6a. The slant lines correspond to waves at 5°S, similar but not identical to those at 5°N in Fig. 6a.

pared with observations at 5°N and 5°S in Figs. 6a and 6b (top and middle panels). These figures use XBT observations (section 2b) to fill in the region near the western boundary that is not observed by the buoys (the boundary between the two datasets is marked by the lines at 165°E in Figs. 6a and 6b). The XBT observations are much more sparsely sampled than the buoys, so the resolution of the signals is relatively poor, with smaller amplitudes; however this is the only method available to observe the thermocline variability in the important western region. Quantities shown in Fig. 6 are demeaned by the 1988–93 mean at each location (unlike the 20°C depths in Fig. 4, which are demeaned by the average annual cycle). Figure 7 shows overlaid time series of model and buoy observations at 5°N and 5°S, 165°E at the west end of the buoy array, where the solution comprises Rossby waves integrated over most of the basin. The correlation between model and buoy observations is 0.89 at 5°N and 0.83 at 5°S for the period 1988–93, suggesting that even as simple a model as (3) represents most of the low-frequency variability at these latitudes (Fig. 7).

c. *Annual cycle and eastern boundary reflections*

The most prominent mode of variability at 5°N and 5°S is the annual Rossby wave, which has been previously described and found to have been generated by interior winds (Meyers 1979; Kessler 1990; Delcroix et al. 1991). Figure 6a shows the observed depth of the 20°C isotherm along 5°N (middle), plotted at the same scale as the model solution (top). The annual Rossby wave is clearly visible in both model and observations as the tilted bands of depth fluctuations, which take about 6 months to propagate from 110°W to 140°E (note that the model solution and the observations at ±5° latitude are plotted with east at the top to facilitate description of western boundary reflection in the next section). The 1991–93 El Niño appears as a weaker-than-usual deep thermocline period during late 1991 in this record. At 5°S (Fig. 6b) the corresponding annual signals are somewhat less clearly defined than north of the equator, probably due to the additional contribution of forcing associated with the annual migration of the intertropical convergence zone (ITCZ) in the Northern Hemisphere (Kessler 1990). The heavy slant lines overlaid on the contour plots at 5° latitude (middle panels) show the time of maximum deepening of the isotherm each year; these lines are drawn with the slope of the theoretically expected long Rossby wave speed ($c_r = \beta c^2/f^2 = 0.81$ m s^{-1}).

Although one might be tempted to infer that the annual Rossby waves in Fig. 6a are propagating from the eastern boundary as the result of Kelvin wave reflection, this is not the case (note that the eastern edge of the buoy data shown in Fig. 6 is at 110°W, about 3600 km west of the South American coast). Figure 8 compares time series of observed 20°C depth at the equator and 5°N, both at 110°W. If eastern-boundary-reflected Rossby waves were the primary process determining thermocline depth variability at 5°N, then these two time series should be well correlated with a 2-month lag to account for the propagation time at the

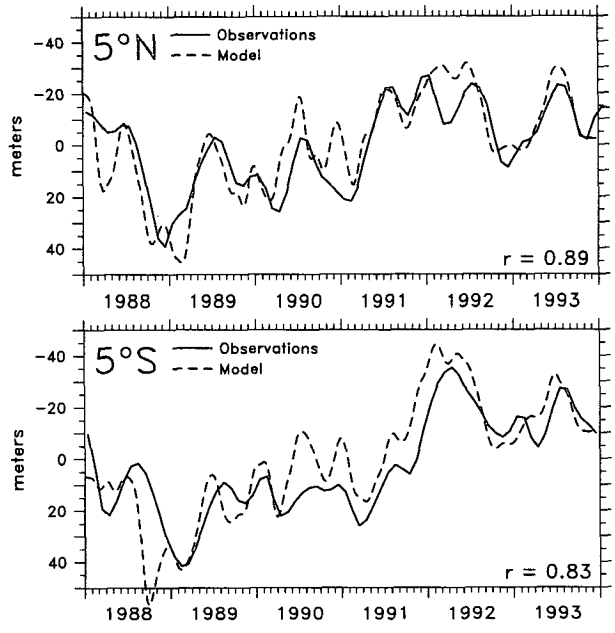

FIG. 7. Comparison of observed (line) and modeled (dash) thermocline depth at 5°N (top) and 5°S (bottom), 165°E, during 1988–93. The correlation between the two time series is shown at lower right.

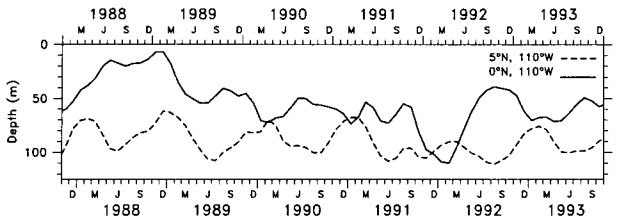

FIG. 8. Time series of 20°C depth (m) at 5°N, 110°W (dashed line) and 0°, 110°W (solid line). The equatorial time series has been lagged 60 days to account for propagation from 0°, 110°W along the equator to the American coast and from the coast along 5°N to 110°W. The two time axes reflect this lag, with the upper time axis for the 5°N time series, and the lower for the lagged equatorial time series.

Kelvin wave speed from the equator, 110°W to the South American coast at 80°W, then at the Rossby wave speed back to 110°W along 5°N. In fact, the timing of lagged equatorial anomalies is almost 180° out of phase with that needed to produce the Rossby waves seen at 5°N by reflection (Fig. 8). The deep phase of the annual cycle at 5°N, 110°W corresponded to the shallow phase at the equator in the middle of each year 1988 through 1993 (Fig. 8). The deep equatorial thermocline peak of the 1991–92 event occurred in January–February 1992 at 0°, 110°W, but this very strong signal was followed by a shoaling Rossby wave at 5°N. Similarly, the shallow equatorial thermocline peak in mid-1992 preceded a downwelling Rossby wave at 5°N later that year (Fig. 8). At the lowest perceptible frequency, the long-term trend of the equatorial time series is seen to move downward during 1988 until 1990, but the 5°N, 110°W time series shows a regular annual cycle with little lower-frequency variation (Fig. 8). At 5°S, the disconnection of the far eastern ocean with the central basin Rossby propagation is similarly clear from the observations shown in Fig. 6b (middle).

The lack of consistency with simple eastern boundary reflection theory between the equator and ±5° latitude agrees with other recent studies that suggest that reflection of equatorial Kelvin waves is only a minor contribution to variability at 5°N, except very near the coast. Delcroix et al. (1991) and du Penhoat et al. (1992) examined Geosat altimeter observations during the 1986–87 El Niño and found an annual Rossby wave similar to those seen in Fig. 6a (middle). Despite some ambiguous examples of possible reflection, they concluded that this mechanism is of secondary importance to wind forcing in the off-equatorial region. Minobe and Takeuchi (1994) studied equatorial waves in the Levitus (1982) climatology and a linear, wind-driven model and showed that the phase of the first meridional mode, first baroclinic mode annual Rossby wave jumps about 180° between the eastern boundary and 120°W in both model and observations, consistent with the out-of-phase relation found here. Kessler (1990) also found that the reflected Rossby wave could only be observed within a few thousand kilometers west of the coast in the 20°C depth field obtained from XBT data. In sum, observations from a variety of sources confirm that eastern boundary reflection plays only a minor role in producing annual variability west of about 120°W. Kessler and McCreary (1993) explained this phenomenon by showing that the reflection of the annual equatorial signal propagated vertically into the subthermocline ocean within a few thousand kilometers of the boundary, and thus effectively disappeared from the upper ocean. The long Rossby model (3) confirms the earlier findings that the annual Rossby wave is wind generated by correctly simulating observed variability (Fig. 7, showing correlations greater than 0.8), with most of the amplitude generated in midbasin and little of the annual amplitude coming from the far east (Figs. 6a and 6b, top).

d. Interannual variability and western boundary reflections

Figure 9 shows observed variability along 5°N, 5°S, and the equator (the same data as in the middle and lower panels of Figs. 6a and 6b) filtered with a 13-month running mean to display the interannual component. Interannual anomalies of 20°C depth were symmetric about the equator, with a deep thermocline in the western two-thirds of the basin from early 1988 until mid-1991 (associated with the strong equatorial easterlies during the La Niña of 1988–89), then shallow in this region with the shift to westerly winds through

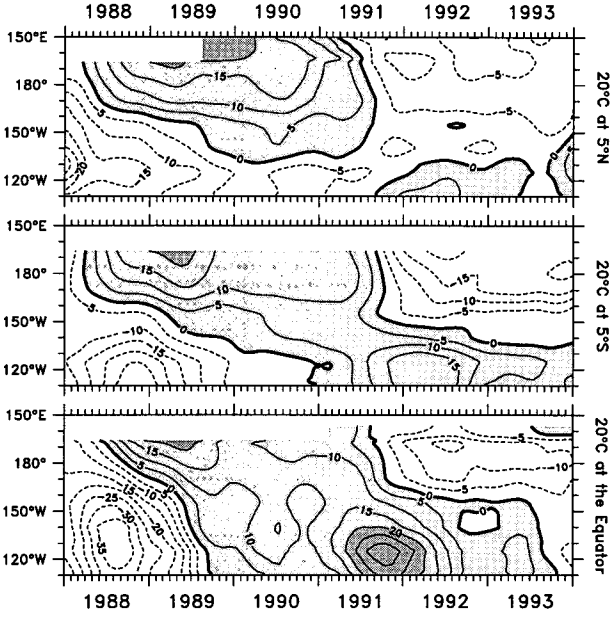

FIG. 9. Observations of 20°C depth at 5°N (top), 5°S (middle), and the equator (bottom), low-pass filtered with a 13-month running mean and demeaned by the 1988–93 mean. Contours are every 5 m, and dark shading indicates deep anomalies.

the end of 1993. These anomalies are also clearly visible as the low-frequency trend superimposed on the regular annual cycles in Figs. 6a and 6b. One might interpret the eastward progression of equatorial deep anomalies from 165°E in early 1989 to the warm event peak in the east in early 1992 (Fig. 9, bottom) as a slow propagation with a speed of about 0.1 m s^{-1}. However, the deep anomalies were interrupted in 1990, which does not support the idea of continuous propagation. In all likelihood, these slow changes indicate a quasi-equilibrium response in the "fast-wave limit" (Neelin 1991) on these timescales.

A different view of the propagation of interannual signals is provided by the monthly time series (Fig. 6a, bottom), in which the deep anomalies of 1991–92 and again in early 1993 appear as roughly 6-month events with a distinct eastward progression, unlike the annual deep signals of the preceding years. Both of these events appeared to have begun near the date line and progressed east at a speed of about 0.6 m s^{-1}. The SST (Fig. 3) and zonal wind (Fig. 2) show that during late 1991 the warmest SST (the 29.5°C patch near the date line) and westerly winds also progressed east at a similar speed for a few months, always lagging west of the thermocline anomalies. This might be an example of the slow coupled propagation referred to by Battisti (1988) and Chao and Philander (1993). Anomalies of zonal wind, thermocline depth, and SST were all about twice as large during the 1991–92 event as during 1993 (Fig. 2, 3, and 4).

To examine the role of western boundary reflection in the evolution of interannual variability, the monthly data plots (Figs. 6a and 6b, middle) have overlaid Rossby speed lines showing the observed deep-thermocline events. These lines connect with hypothetical Kelvin wave paths on the equator showing the Kelvin waves that would be expected to result from western boundary reflection (steeper lines in Figs. 6a and 6b, bottom). The generally poor match of the predicted Kelvin waves with equatorial thermocline depth observations shows that theoretical linear western boundary reflection of anomalies at ±5° latitude did not often correspond to subsequent observed variability on the equator. In fact, the equatorial sequelae of most of the downwelling Rossby waves during this period was the opposite of what would have been expected from western boundary reflection. The deep off-equatorial Rossby signals in early 1990, 1991, and 1993 all preceded shallow equatorial signals along the predicted wave path (Fig. 6a and 6b).

The overall impression from Figs. 6a and 6b is that western boundary reflection usually is not the major determinant of equatorial variability far from the boundary. In the few cases where the Rossby signals were especially strong (the downwelling in early 1989 and the upwelling in early 1992; possibly also an upwelling event in late 1988), the reflected signals can be seen into midbasin; however, both of these encountered unfavorable winds that caused a steady erosion of amplitude. This situation is to be expected, since if the wind anomaly that generates a Rossby wave persists during the time it takes the wave to propagate to the boundary and return to the same longitude as a Kelvin wave (about 125 days for an equatorial wind signal at 160°W), the winds will then oppose the wave-induced anomalies and tend to erode it. As equatorial Pacific wind anomalies commonly do last for at least this long (Fig. 2), the lack of clear signatures of western boundary reflection in observed equatorial thermocline depth variability is not surprising.

On the other hand, the downwelling Rossby wave, which arrived at the western boundary in early 1989 following the 1988 La Niña, was the largest downwelling anomaly, by perhaps a factor of 2, during the study period (Figs. 6a and 6b, middle). Both the long Rossby model and the XBT observations suggest that while the other downwelling events appear to have weakened near the boundary, the 1989 signal grew in intensity west of the region where buoy observations are available, (Figs. 6a and 6b, top and middle), due to the anomalous La Niña easterlies in the far west (Fig. 2). This large wave did produce a downwelling equatorial Kelvin wave consistent with linear western boundary reflection, and the Kelvin wave carried the deep-thermocline signal at least to 140°W (Figs. 6a and 6b, bottom). The equatorial deepening along the wave path cannot be attributed to local wind forcing, since the observed west Pacific equatorial winds were still strongly easterly until November 1989 (Fig. 2).

It appears from Figs. 6a and 6b that both the Wyrtki (1975) buildup hypothesis and delayed oscillator theory would have led one to expect a warm event to begin in 1989 or 1990 (associated with the strong reflected downwelling wave), and at the time many observers felt that an El Niño was developing (Kerr 1990). Indeed, SST warmed and westerly winds developed near the date line at the end of 1989 (Figs. 2 and 3), but it was not until 1991 that the event got underway according to the traditional definition of large SST anomalies in the east (Fig. 3). The lag between the initiation of downwelling in the west and the occurrence of El Niño was more than two years (Fig. 9, bottom), and equatorial variability during this period showed two strong seasonal cycles (Figs. 6a and 6b), with anomalies of both signs. In this light it is difficult to attribute the 1991–92 event to the 1989 Rossby wave train via the delayed oscillator mechanism. Neither the buildup nor the delayed oscillator hypotheses appear to satisfactorily explain the evolution of variability in the equatorial Pacific during 1989–91. It may be that the delay between downwelling Rossby reflection and the appearance of warm anomalies in the eastern Pacific depends on the intensity of the previous La Niña (Clarke and Li 1994). The unusually shallow thermocline and cold SST anomalies in the eastern equatorial Pacific during 1988–89 would be consistent with

this hypothesis. Alternately, it has been suggested that the delayed oscillator theory applies most compellingly to the termination of warm events, and the arrival of even very large downwelling Rossby waves in the west should not be considered a sufficient trigger on its own for the onset of El Niño (Mantua and Battisti 1994).

In particular, the very large equatorial thermocline deepening at the end of 1991, which defined the 1991–92 El Niño, was not a direct reflection of a Rossby wave. The long Rossby model results (Figs. 6a and 6b, top) show that the Rossby wave wind forcing was close to normal during 1990 and early 1991, and in accord with the usual annual cycle, a moderate downwelling Rossby wave arrived in the west in early April 1991 (Figs. 6a and 6b, middle). The XBT observations suggest that this wave lost amplitude west of 165°E, and the wind-forced model also tends to confirm the weakening of the 1991 downwelling wave in the far west. Thermocline variability on the equator along the expected path of this signal showed no sign of downwelling, which might be expected following reflection (Fig. 6a, bottom), and this is confirmed by the Kelvin wave model (1) (section 3b), which reproduced the observed equatorial thermocline depth variations at this time with interior winds alone (Fig. 5). The actual El Niño deepening began about four months later in late August 1991, at a time when the forcing emanating from the western boundary was weak or upwelling favorable. In the intervening months, the thermocline in the west was quite close to seasonally normal (Fig. 4, bottom), and SST was about 0.5°C anomalously warm across the same broad region (Fig. 3, bottom), neither of which appears correlated with western boundary reflected signals. It is therefore difficult to find a connection between the rather typical annual downwelling Rossby wave of early 1991 and the subsequent initiation of the 1991–92 El Niño.

Once the El Niño was underway in late 1991, strong equatorial westerly winds favored generation of upwelling Rossby waves, and both model and observations show development of a shallow thermocline off the equator in the western half of the basin (Figs. 6a and 6b, top and middle). This led to a major disruption in the usual annual downwelling Rossby wave that would have been expected to arrive in the west at the beginning of 1992, and the shallow anomalies seen west of about 160°W at ±5° latitude were very strongly anomalous for that time of year (the thermocline was about 40 m higher than it had been at the same time one year before) (Figs. 6a and 6b, middle). We showed in section 3b (see the discussion of Fig. 5) that although interior wind-generated Kelvin waves accounted very well for observed variability on the equator in the central Pacific during the deepening stage of the 1991–92 El Niño, this interior forcing did not explain the strong shoaling that terminated the event. However, upwelling Rossby waves produced by westerlies at the height of the warm event appeared to have reached the western boundary in early 1992 and reflected as an upwelling Kelvin wave at just the right time to produce the observed, otherwise unaccounted for, shoaling at 140°W (dashed lines in Fig. 6a and 6b, middle and bottom). The equatorial winds continued to be anomalously westerly until mid-1992 (Fig. 2), so this upwelling could not have been produced on the equator. Although the buoys do not extend to the western boundary, leaving the possibility that winds west of 165°E could have caused the upwelling, we checked this using the Kelvin wave model (1), forced with FSU monthly winds, which extend over the entire basin to 124°E. The model results confirm that equatorial winds west of 165°E did not produce the upwelling signal. We conclude that the process that terminated the 1991–92 El Niño occurred by western boundary reflection of shallow off-equatorial signals generated during the warm event peak, as predicted by delayed oscillator theory. By boreal fall 1992, the equatorial thermocline ranged from near-normal depths in the east to about 20 m anomalously shallow in the west (Fig. 4).

As the 1991–92 El Niño terminated and the equatorial thermocline shoaled, cool SST anomalies also appeared in the cold tongue region during the latter half of 1992 (Fig. 10). However, these cool anomalies did not extend poleward of a few degrees latitude or west of about 160°W. Rather than presaging the development of a La Niña event, like that which followed the 1986–87 El Niño, the strong cold tongue of late 1992 subsequently weakened and gave way to a new outbreak of basin-scale warm anomalies in early 1993. The 1993 warm event occurred with the west Pacific thermocline still about 20 m anomalously shallow (Fig. 4), which directly contradicts the idea that a "buildup" of a thick warm layer is prerequisite to an El Niño. Considering the role of western boundary reflection in the onset of the 1993 event, we find that both the long Rossby model and thermocline depth observations at 5°N and 5°S show only upwelling signals arriving at the western boundary until at least the end of 1992 and into 1993 (Figs. 6a and 6b, top and middle), consistent with the continuation of equatorial westerly

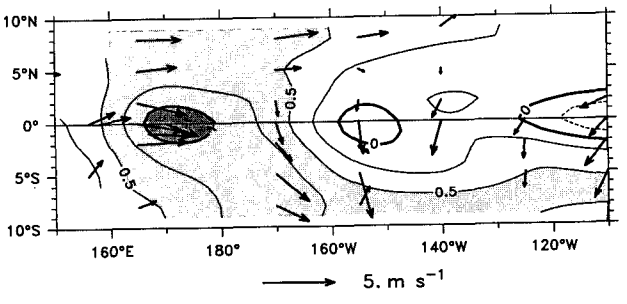

FIG. 10. SST and wind anomalies during September 1992. Contours of SST anomalies are drawn every 0.25°C, with shading for warm anomalies greater than 0.5°C and 1°C. Wind vectors begin at the buoy positions. A 5 m s^{-1} scale vector is shown at bottom.

winds over at least the western half of the basin (Fig. 2). Therefore, there is no mechanism for producing the equatorial thermocline deepening seen in the early months of 1993 by boundary reflection. As in the case of the first warm event peak roughly one year earlier, thermocline depth anomalies during the onset of the 1993 El Niño were due entirely to interior winds (Fig. 5).

At the end of 1992, as the 1993 warm event was about to begin, the thermocline was anomalously shallow, particularly in the west (Fig. 4), SST near the date line was about 1°C anomalously warm (Fig. 10), and anomalous westerlies extended over the western part of the basin (Fig. 10). Thermocline deepening began near the date line and propagated eastward in a few Kelvin pulses (Fig. 4), with the overall signal moving at about 0.6 m s^{-1}; the monthly average thermocline anomalies appeared quite similar to those of the earlier 1991–92 warming (Fig. 6a, bottom). These circumstances might seem to be partly consistent with the coupled instability element of the delayed oscillator mechanism producing a brief warm event independent of western boundary reflections. In this scenario, the unusually warm SSTs near the date line would enhance low-level convergence in the atmosphere, reinforcing westerly wind anomalies in this region and to the west (Fig. 10). These westerlies would in turn favor intensification and eastward spread of warm SSTs through both eastward advection and thermocline downwelling. We note that a series of strong intraseasonal Madden–Julian oscillations occurred in the western equatorial Pacific during late 1992–early 1993 (these westerly events are seen in Fig. 2). Surface westerly winds associated with these oscillations excited equatorial Kelvin waves observed both in the TAO dataset (Fig. 4) and the Topography Experiment (TOPEX)/Poseidon altimeter (Busalacchi et al. 1994). It appears that the combined effect of the series of downwelling waves lowered the east Pacific thermocline to the point where SST warmed because local upwelling was unable to cool the surface (KM). This warming in turn may have favored the appearance of westerlies across the eastern Pacific in early 1993.

5. Summary and conclusions

Surface wind and upper-ocean thermal structure associated with the 1991–93 El Niño were observed better than during any previous warm event. The highly resolved temporal sampling showed that the interannual variations were composed of a series of higher-frequency events, prominently at the 60-day Madden–Julian timescale (Kessler et al. 1995). Westerly winds and convection oscillating at this frequency, which are usually confined west of the date line, penetrated into the central Pacific in concert with warm SST and generated large-amplitude downwelling equatorial Kelvin waves that carried this signal to the eastern part of the ocean. At 140°W each of the downwelling waves lowered the thermocline 40–50 m.

A simple model consisting only of first and second baroclinic mode Kelvin waves forced by zonal winds between 165°E and 140°W was used to examine 20°C depth variations along the equator during 1991–93. It was not possible to unambiguously determine the relative importance of the first two baroclinic mode Kelvin waves in this model, primarily because the main forcing region was in the central Pacific and the modes did not have time to disperse. However, in agreement with earlier studies, vertical modes higher than the second were found not to have made a significant contribution to upper-ocean thermal variations.

This Kelvin wave model agreed well with observed thermocline variations during the onset phase of the 1991–92 warm event (Fig. 5). During the year leading up the El Niño peak in February 1992, the model hindcast observed thermocline motions with a correlation near 0.9, showing that the thermocline in the east-central Pacific was controlled largely by interior winds, primarily in the region near the date line. Both the intraseasonal waves and the lower-frequency thermocline downwelling signals were well simulated. At this time, forcing originating in Rossby waves arriving at the western boundary was weak, and the El Niño onset deepening in late August 1991 was not due to a western boundary reflected signal. However, the Kelvin wave model did not reproduce the thermocline shoaling that represented the end of the 1991–92 event in mid-1992. The interior-basin winds were continued to be anomalously westerly or near normal while the thermocline rose rapidly and the event terminated. This shoaling was instead apparently associated with reflection at the western boundary of upwelling Rossby waves generated by westerlies in the central Pacific during the peak warm period, as suggested by delayed oscillator theory. During late 1992 and early 1993 when the second, weaker warm event occurred, western boundary forcing was again small, and the Kelvin wave model forced only with interior winds hindcast the thermocline deepening accurately. However, as in 1992, the interior winds indicated a continued deepening in mid-1993, but instead the observed thermocline shoaled as the second warm event ended.

Three distinct speeds of eastward progression of anomalies along the equator were noted. With minimal smoothing (Fig. 4) the oceanic free Kelvin wave speed ($c \approx 2.5$ m s^{-1}) is evident in the propagation of intraseasonal-frequency signals. In the monthly average plots (Fig. 6a, bottom), intraseasonal waves are largely filtered out and the 6-month envelopes of ENSO thermocline depth anomalies are seen to have arisen near the date line and moved east at a speed of about 0.6 m s^{-1} during both the 1991–92 and 1993 events. When the same data are filtered with a 13-month running mean (Fig. 9, bottom), 20°C depth anomalies appear to have moved from 165°E in early 1989 to 110°W in

late 1991 at a speed of about 0.1 m s^{-1}, although the observations do not seem to represent a continuous propagation at this speed. This slow signal was found to have relatively large meridional extent, being quite similar everywhere between 5°N and 5°S (Fig. 9), unlike the two faster speeds noted that were seen only close to the equator, with little or no expression at 5° latitude. The two slower speeds must represent coupled phenomena, but determination of the nature of these signals will require study of a coupled model and is beyond the scope of this paper.

In general, western boundary reflection appeared not to be the major determinant of variability on the equator, except for a few cases where the Rossby signals were especially large (the downwelling wave due to the La Niña of 1988 and the upwelling wave produced by the El Niño of 1991–92). The Rossby waves could be clearly traced, but subsequent equatorial signals were usually not consistent with the Kelvin waves that would have been predicted by simple western boundary reflection theory. In particular, the origin of the 1991–92 and 1993 events could not be found in signals due to western boundary reflection. However, the termination of the 1991–92 El Niño can only be explained as a result of the reflection of the upwelling wave generated by westerlies during the height of the warm event.

Along 5°N latitude the most prominent mode of variability was the annual Rossby wave, which has been previously studied by several investigators; this wave was found to be generated by interior winds, with little influence of eastern boundary Kelvin wave reflection. The large-amplitude El Niño signals in the eastern equatorial Pacific similarly did not produce reflected Rossby waves that could be observed in midbasin. In fact, the Rossby waves seen off the equator subsequent to the equatorial events were of the opposite sign to what would have been expected from eastern boundary reflection. During early 1992, the equatorial anomaly arriving at the eastern boundary was a strong deepening associated with the height of the warm event, but the subsequent observed signature at 5°N was instead an upwelling Rossby wave clearly associated with the interior wind stress anomalies. Similarly, the equatorial shoaling of mid-1992 was followed by a downwelling, wind-generated Rossby wave at 5°N. At 5°S in the far eastern Pacific, variability somewhat more consistent with eastern boundary reflection of the largest signals was observed, but again the waves apparently did not penetrate farther west than about 120°W. These observations agree with earlier studies suggesting that such Rossby waves would propagate vertically into the subthermocline ocean east of the buoy array. Interannual variability off the equator was seen as a deepening of the thermocline everywhere west of about 140°W associated with the 1988–89 La Niña, followed by shoaling as westerly wind anomalies began to occur over the equatorial region during 1990 and 1991. The swing from deep to shallow thermocline amounted to about 40-m-depth change of the 20°C isotherm in about three years.

An evaluation of the delayed oscillator mechanism in relation to the 1991–93 events showed a longer lag between the arrival of an interannual downwelling Rossby wave in the western Pacific in 1989 and the subsequent initiation of El Niño than had been previously seen in model simulations (Wakata and Sarachik 1991a). Following the strong downwelling signal due to Rossby waves from the La Niña of 1988–89, many observers had noted the deepening of the west Pacific and expected the occurrence of a warm event in 1990. Westerly winds and warm SST were observed in the west during 1990 and 1991, and this forcing led to some shoaling of the thermocline in that region, partially reducing the buildup of warm water in the west well before the 1991–92 event. However, the Zebiak and Cane (1987) model correctly predicted both the nonoccurrence of an El Niño in 1990 and the actual onset in late 1991 of the 1991–92 El Niño. The success of this model suggests that a thorough diagnosis of these correct predictions would be worthwhile in identifying the role played by delayed oscillator dynamics. It is worth noting in this context that this early (January 1991) (Climate Analysis Center 1991) forecast suggests that the eruption of Mt. Pinatubo in the Philippines in July 1991 was probably not the trigger for the event, as has been suggested by volcanoes-cause-El Niño enthusiasts [for a discussion of both sides of this issue, see Handler and Ansager (1990) and Nicholls (1990)].

A downwelling Rossby wave fairly typical of the usual annual cycle arrived at the western boundary in early 1991 but did not produce a significant Kelvin wave–reflected signal in the central basin, and the Kelvin model confirms that equatorial thermocline depth variability during 1991 at 140°W was due entirely to interior winds, not boundary reflection. The actual El Niño deepening began about four months later, in late August 1991, at a time when no western boundary–generated Kelvin waves were observed. During the intervening period leading up to the onset of El Niño anomalies, zonal winds were close to normal (Fig. 2), SST was slightly anomalously warm, primarily in the east (Fig. 3), and 20°C depth was within about 10 m of seasonal normals and slightly shallow in the west (Fig. 4). In the west Pacific none of these quantities appeared connected to reflected Rossby signals. Although the precursors to the event presumably existed in the Pacific during early 1991 (since the Zebiak and Cane model correctly predicted the onset), we are unable to point to any obvious features of the observed oceanic conditions that unambiguously foretold the oncoming episode, except possibly the modest SST anomalies. It may be that the broadly warmer SST tended to enhance the seasonal westerlies over the western Pacific when they appeared in late boreal sum-

mer 1991. In addition, KM found that the initial SST warming event in September 1991 occurred simultaneously across at least 8000 km of zonal extent, faster than any propagation that could be due to oceanic waves. This suggests that further modification of theories of the ENSO cycle may be necessary to take into account such extremely rapid processes.

The warm event seemed to end in boreal fall 1992 with a strong return of the cold tongue in the east and shallow thermocline in the western equatorial Pacific. The termination could not be accounted for by waves forced by interior equatorial winds and apparently was due to reflection of an upwelling Rossby wave generated during the event, just as predicted by delayed oscillator theory. However, despite the persistent shallow thermocline in the west, in early 1993 a second warm event occurred, with SST anomalies greater than 1.5°C at 110°W. One factor that may have been crucial in the reoccurrence of warming in 1993 was that SST near the date line remained anomalously warm through 1992, and this may have fostered the advance of convection and westerly winds into the central basin. While we cannot explain at present why the second episode took place, the fact of a warm event while the upper layer in the west was quite anomalously shallow implies that the Wyrtki (1975) buildup paradigm is not necessarily an essential feature of the ENSO phenomenon. Also, that the 1993 warm event occurred without a downwelling equatorial Rossby wave precursor implies that the ENSO cycle cannot be simply viewed as an oscillator mediated by propagation and reflection of equatorial Rossby waves.

Acknowledgments. We thank Klaus Weickmann and Allan Clarke for thoughtful comments on an earlier version of this manuscript. Dai McClurg of NOAA/PMEL helped in processing the buoy temperature data and gave expert assistance with graphics. Jerry Davison of NOAA/PMEL processed the COADS wind and SST climatologies. Gridded ship wind data were provided by David Legler and Jim O'Brien of FSU. The weekly satellite blended SST fields were produced by Dick Reynolds, Diane Stokes, and Thomas Smith at the National Centers for Environmental Prediction. Jay McCreary wrote the program to decompose the density profile into vertical modes. Support from NOAA's Equatorial Pacific Ocean Climate Studies and Tropical Ocean/Global Atmosphere programs is gratefully acknowledged.

REFERENCES

Anderson, D. L. T., and J. P. McCreary, 1985: Slowly propagating disturbances in a coupled ocean–atmosphere model. *J. Atmos. Sci.*, **42**, 615–629.

Battisti, D. S., 1988: The dynamics and thermodynamics of a warm event in a coupled atmosphere/ocean model *J. Atmos. Sci.*, **45**, 2889–2919.

——, 1989: On the role of off-equatorial Rossby waves during ENSO. *J. Phys. Oceanogr.*, **19**, 551–559.

——, and A. C. Hirst, 1989: Interannual variability in a tropical ocean–atmosphere model: Influence of the basic state, ocean geometry and nonlinearity. *J. Atmos. Sci.*, **46**, 1687–1712.

——, and E. S. Sarachik, 1995: Understanding and predicting ENSO. U.S. National Report to Int. Union of Geodesy and Geophys.: Contributions in Oceanography, in press.

Bjerknes, J., 1966: A possible response of the atmospheric Hadley circulation to equatorial anomalies of ocean temperature. *Tellus*, **18**, 820–829.

Busalacchi, A. J., and J. J. O'Brien, 1980: The seasonal variability in a model of the tropical Pacific. *J. Phys. Oceanogr.*, **10**, 1929–1951.

——, and ——, 1981: Interannual variability of the equatorial Pacific in the 1960's. *J. Geophys. Res.*, **86**, 10 901–10 907.

——, and M. A. Cane, 1985: Hindcasts of sea level variations during the 1982–83 El Niño. *J. Phys. Oceanogr.*, **15**, 213–221.

——, M. J. McPhaden, and J. Picaut, 1994: Variability in equatorial Pacific sea surface topography during the verification phase of the TOPEX/Poseidon Mission. *J. Geophys. Res.*, **99**, 24 725–24 738.

Cane, M. A., 1984: Modeling sea level during El Niño. *J. Phys. Oceanogr.*, **14**, 1864–1874.

——, and E. S. Sarachik, 1977: Forced equatorial ocean motions. II. The linear equatorial bounded case. *J. Mar. Res.*, **35**, 395–432.

——, and P. R. Gent, 1984: Reflection of low-frequency equatorial waves at arbitrary western boundaries. *J. Mar. Res.*, **42**, 487–502.

——, S. E. Zebiak, and S. C. Dolan, 1986: Experimental forecasts of El Niño. *Nature*, **322**, 827–832.

Chang, P., and S. G. H. Philander, 1989: Rossby wave packets in baroclinic mean currents. *Deep-Sea Res.*, **36**, 17–37.

Chao, Y., and S. G. H. Philander, 1993: On the structure of the Southern Oscillation. *J. Climate*, **6**, 450–469.

Clarke, A. J., 1983: The reflection of equatorial waves from oceanic boundaries. *J. Phys. Oceanogr.*, **13**, 1193–1207.

——, 1992: Low-frequency reflection from a nonmeridional eastern ocean boundary and the use of coastal sea level to monitor eastern Pacific equatorial Kelvin waves. *J. Phys. Oceanogr.*, **22**, 163–183.

——, 1994: Why are surface equatorial ENSO winds anomalously westerly under anomalous large-scale convection? *J. Climate*, **7**, 1623–1627.

——, and B. Li, 1994: On the amplitude and timing of warm and cold El Niño/Southern Oscillation events. *J. Climate*, submitted.

Climate Analysis Center, 1991: Climate Diagnostics Bulletin, Near Real-time Analyses, January 1991. U.S. Dept. of Commerce, Natl. Oceanic and Atmos. Administration, Washington, DC.

Delcroix, T., J. Picaut, and G. Eldin, 1991: Equatorial Kelvin and Rossby waves evidenced in the Pacific Ocean through Geosat sea level and surface current anomalies. *J. Geophys. Res.*, **96** (Supp.), 3249–3262.

du Penhoat, Y., T. Delcroix, and J. Picaut, 1992: Interpretation of Kelvin/Rossby waves in the equatorial Pacific from model-Geosat data intercomparison during the 1986–1987 El Niño. *Oceanol. Acta*, **15**, 545–554.

Enfield, D. B., 1987: The intraseasonal oscillation in eastern Pacific sea levels: How is it forced? *J. Phys. Oceanogr.*, **17**, 1860–1876.

Giese, B. S., and A. J. Clarke, 1974: Wind-induced upwelling, coastal currents and sea-level changes. *Deep-Sea Res.*, **21**, 325–345.

——, and D. E. Harrison, 1990: Aspects of the Kelvin wave response to episodic wind forcing. *J. Geophys. Res.*, **95**, 7289–7312.

Godfrey, J. S., 1975: On ocean spindown. Part I: A linear experiment. *J. Phys. Oceanogr.*, **5**, 399–409.

Handler, P., and K. Ansager, 1990: Volcanic aerosols, El Niño and the Southern Oscillation. *Intl. J. Climatol.*, **10**, 413–424.

Hayes, S. P., L. J. Mangum, J. Picaut, A. Sumi, and K. Takeuchi, 1991: TOGA-TAO: A moored array for real-time measurements in the tropical Pacific Ocean. *Bull. Amer. Meteor. Soc.*, **72**, 339–347.

Kerr, R. A., 1990: Who will win the El Niño sweepstakes this time? *Science,* **248,** p. 445.

Kessler, W. S., 1989: Observations of long Rossby waves in the northern tropical Pacific. PMEL Tech. Memo. ERL PMEL-86, 169 pp.

——, 1990: Observations of long Rossby waves in the northern tropical Pacific. *J. Geophys. Res.,* **95,** 5183–5217.

——, 1991: Can reflected extra-equatorial Rossby waves drive ENSO? *J. Phys. Oceanogr.,* **21,** 444–452.

——, and B. A. Taft, 1987: Dynamic heights and zonal geostrophic transports in the central tropical Pacific during 1974–84. *J. Phys. Oceanogr.,* **17,** 97–122.

——, and J. P. McCreary, 1993: The annual wind-driven Rossby wave in the subthermocline equatorial Pacific. *J. Phys. Oceanogr.,* **23,** 1192–1207.

——, and M. J. McPhaden, 1995: El Niño of 1991–93 in the central Pacific. *Deep-Sea Res.,* in press.

——, ——, and K. M. Weickmann, 1995: Forcing of intraseasonal Kelvin waves in the equatorial Pacific. *J. Geophys. Res.,* in press.

Kubota, M., and J. J. O'Brien, 1988: Variability of the upper tropical Pacific Ocean model. *J. Geophys. Res.,* **93,** 13 930–13 940.

Legler, D. M., 1991: Producing surface wind products for oceanographers. *Proc. IGOSS/IOC Ocean Products Workshop,* Tokyo, Japan, Intergovernmental Oceanic Commission, 59–76.

Levitus, S., 1982: *Climatological Atlas of the World Ocean.* NOAA Prof. Paper 13, 173 pp.

Lukas, R., S. P. Hayes, and K. Wyrtki, 1984: Equatorial sea level response during the 1982–83 El Niño. *J. Geophys. Res.,* **89,** 10 425–10 430.

Madden, R. A., and P. R. Julian, 1971: Detection of a 40–50 day oscillation in the zonal wind in the tropical Pacific. *J. Atmos. Sci.,* **28,** 702–708.

——, and ——, 1972: Description of global-scale circulation cells in the tropics with a 40–50 day period. *J. Atmos. Sci.,* **29,** 1109–1123.

Mantua, N. J., and D. S. Battisti, 1994: Evidence for the delayed oscillator mechanism for ENSO: The "observed" oceanic Kelvin mode in the far western Pacific. *J. Phys. Oceanogr.,* **24,** 691–699.

McCreary, J. P., 1981: A linear stratified ocean model of the equatorial undercurrent. *Philos. Trans. Roy. Soc. London Ser. A,* **278,** 603–635.

——, 1983: A model of tropical ocean–atmosphere interaction. *Mon. Wea. Rev.,* **111,** 370–387.

——, 1984: Equatorial beams. *J. Mar. Res.,* **42,** 395–430.

——, and D. L. T. Anderson, 1991: An overview of coupled ocean–atmosphere models of El Niño and the Southern Oscillation. *J. Geophys. Res.,* **96,** 3125–3150.

McPhaden, M. J., 1993: TOGA-TAO and the 1991–93 El Niño-Southern Oscillation event. *Oceanography,* **6,** 36–44.

Meyers, G., 1979: On the annual Rossby wave in the tropical North Pacific Ocean. *J. Phys. Oceanogr.,* **9,** 663–674.

——, and J.-R. Donguy, 1980: An XBT network with merchant ships. *Trop. Ocean-Atmos. Newslett.,* **2,** 6–7.

Minobe, S., and K. Takeuchi, 1994: Annual period equatorial waves in the Pacific Ocean. *J. Geophys. Res.,* submitted.

Moore, D. W., and S. G. H. Philander, 1977: Modeling of the tropical oceanic circulation. *The Sea.* Vol. 6, E. D. Goldberg, Ed., Wiley-Interscience, 319–361.

Neelin, J. D., 1991: The slow sea surface temperature mode and the fast-wave limit: Analytic theory for tropical interannual oscillations and experiments in a hybrid coupled model. *J. Atmos. Sci.,* **48,** 584–606.

Nicholls, N., 1990: Low-latitude volcanic eruptions and the El Niño/Southern Oscillation: A reply. *Intl. J. Climatol.,* **10,** 425–429.

Penland, C., and T. Magorian, 1993: Prediction of Niño 3 sea surface temperatures using linear inverse modeling. *J. Climate,* **6,** 1067–1076.

——, and L. Matrosova, 1994: A balance condition for stochastic numerical models with application to the El Niño–Southern Oscillation. *J. Climate,* **7,** 1352–1372.

——, and P. D. Sardeshmukh, 1995: The optimal growth of tropical sea surface temperature anomalies. *J. Climate,* in press.

Philander, S. G. H., T. Yamagata, and R. C. Pacanowski, 1984: Unstable air–sea interactions in the tropics. *J. Atmos. Sci.,* **41,** 604–613.

Picaut, J., C. Menkes, J.-P. Boulanger, and Y. du Penhoat, 1993: Dissipation in a Pacific equatorial long wave model. *TOGA Notes,* **10,** 11–15.

Rebert, J. P., J. R. Donguy, G. Eldin, and K. Wyrtki, 1985: Relations between sea level, thermocline depth, heat content and dynamic height in the tropical Pacific Ocean. *J. Geophys. Res.,* **90,** 11 719–11 725.

Reynolds, R. W., and T. M. Smith, 1994: Improved global sea surface temperature analyses using optimal interpolation. *J. Climate,* **7,** 929–948.

Rui, H., and B. Wang, 1990: Development characteristics and dynamic structure of tropical intraseasonal convection anomalies. *J. Atmos. Sci.,* **47,** 357–379.

Schopf, P. S., D. L. T. Anderson, and R. Smith, 1981: Beta-dispersion of low-frequency Rossby waves. *Dyn. Atmos. Oceans,* **5,** 187–214.

Spillane, M. C., D. B. Enfield, and J. S. Allen, 1987: Intraseasonal oscillations in sea level along the west coast of the Americas. *J. Phys. Oceanogr.,* **17,** 313–325.

Springer, S., M. J. McPhaden, and A. J. Busalacchi, 1990: Oceanic heat content variability in the tropical Pacific during the 1982–83 El Niño. *J. Geophys. Res.,* **95,** 22 089–22 102.

Suarez, M. J., and P. S. Schopf, 1988: A delayed action oscillator for ENSO. *J. Atmos. Sci.,* **45,** 549–566.

Wakata, Y., and E. S. Sarachik, 1991a: On the role of equatorial ocean modes in the ENSO cycle. *J. Phys. Oceanogr.,* **21,** 434–443.

——, and ——, 1991b: Unstable coupled atmosphere–ocean basin modes in the presence of a spatially varying basic state. *J. Atmos. Sci.,* **48,** 2060–2077.

Weickmann, K. M., and S. J. S. Khalsa, 1990: The shift of convection from the Indian Ocean to the western Pacific Ocean during a 30–60 day oscillation. *Mon. Wea. Rev.,* **118,** 964–978.

——, G. R. Lussky, and J. E. Kutzbach, 1985: Intraseasonal (30–60 day) fluctuations of outgoing longwave radiation and 250 mb streamfunction during northern winter. *Mon. Wea. Rev.,* **113,** 941–961.

Woodruff, S. D., R. J. Slutz, R. L. Jenne, and P. M. Steurer, 1987: A Comprehensive Ocean–Atmosphere Data Set. *Bull. Amer. Meteor. Soc.,* **68,** 1239–1250.

Wyrtki, K., 1975: El Niño: The dynamic response of the equatorial Pacific to atmospheric forcing. *J. Phys. Oceanogr,* **5,** 572–584.

——, and B. Kilonsky, 1984: Mean water and current structure during the Hawaii-to-Tahiti shuttle experiment. *J. Phys. Oceanogr.,* **14,** 242–254.

Yamagata, T., 1985: Stability of a simple air–sea coupled model in the tropics. *Coupled Ocean–Atmosphere Models,* J. C. J. Nihoul, Ed., Elsevier, 637–656.

Zebiak, S. E., and M. A. Cane, 1987: A model El Niño–Southern Oscillation. Mon. Wea. Rev, **115,** 2262–2278.